12-2-2013

Intensity-demodulated fiber-ring laser sensor system for acoustic emission detection

Ming Han
University of Nebraska-Lincoln, mhan3@unl.edu

Tongqing Liu
University of Nebraska-Lincoln

Lingling Hu
University of Nebraska-Lincoln

Qi Zhang
University of Nebraska-Lincoln

Intensity-demodulated fiber-ring laser sensor system for acoustic emission detection

Ming Han,* Tongqing Liu, Lingling Hu, and Qi Zhang

Department of Electrical Engineering, University of Nebraska-Lincoln, Lincoln, Nebraska, 68588, USA
mhan3@unl.edu

Abstract: We theoretically and experimentally demonstrate a fiber-optic ultrasonic sensor system based on a fiber-ring laser whose cavity consisting of a regular fiber Bragg grating (FBG) and a tunable optical band-pass filter (TOBPF). The FBG is the sensing element and the TOBPF is used to set the lasing wavelength at a point on the spectral slope of the FBG. The ultrasonic signal is detected by the variations of the laser output intensity in response to the cold-cavity loss modulations from the ultrasonically-induced FBG spectral shift. The system demonstrated here has a simple structure and low cost, making it attractive for acoustic emission detection in structure health monitoring.

OCIS codes: (060.2370) Fiber optics sensors; (060.3735) Fiber Bragg gratings; (060.3510) Lasers, fiber; (120.4290) Nondestructive testing.

References and links

1. I. M. Perez, H. L. Cui, and E. Udd, "Acoustic emission detection using fiber Bragg gratings," Proc. SPIE **4328**, 209–215 (2001).
2. P. Fomitchov and S. Krishnaswamy, "Response of a fiber Bragg grating ultrasonic sensor," Opt. Eng. **42**(4), 956–963 (2003).
3. Y. Qiao, Y. Zhou, and S. Krishnaswamy, "Adaptive demodulation of dynamic signals from fiber Bragg gratings using two-wave mixing technology," Appl. Opt. **45**(21), 5132–5142 (2006).
4. H. Tsuda, K. Kumakura, and S. Ogihara, "Ultrasonic sensitivity of strain-insensitive fiber Bragg grating sensors and evaluation of ultrasound-induced strain," Sensors (Basel) **10**(12), 11248–11258 (2010).
5. T. Q. Liu and M. Han, "Analysis of π-phase-shifted fiber Bragg gratings for ultrasonic detection," IEEE Sens. J. **12**(7), 2368–2373 (2012).
6. H. Tsuda, "Bragg wavelength-insensitive fiber Bragg grating ultrasound detection system based on a fiber ring laser," Proc. SPIE **7753**, 77538J (2011).
7. H. Tsuda, "Strain-insensitive fiber Bragg grating ultrasonic sensing system using fiber ring laser," *presented in 18th International Conference on Composite Materials* Jeju Island, South Korea, 2011).
8. D. Gatti, G. Galzerano, D. Janner, S. Longhi, and P. Laporta, "Fiber strain sensor based on a π-phase-shifted Bragg grating and the Pound-Drever-Hall technique," Opt. Express **16**(3), 1945–1950 (2008).
9. A. Rosenthal, D. Razansky, and V. Ntziachristos, "High-sensitivity compact ultrasonic detector based on a π-phase-shifted fiber Bragg grating," Opt. Lett. **36**(10), 1833–1835 (2011).
10. Q. Wu and Y. Okabe, "High-sensitivity ultrasonic phase-shifted fiber Bragg grating balanced sensing system," Opt. Express **20**(27), 28353–28362 (2012).
11. T. A. Guo, A. C. L. Wong, W. S. Liu, B. O. Guan, C. Lu, and H. Y. Tam, "Beat-frequency adjustable Er3+-doped DBR fiber laser for ultrasound detection," Opt. Express **19**(3), 2485–2492 (2011).
12. L. Y. Shao, S. T. Lau, X. Y. Dong, A. P. Zhang, H. L. W. Chan, H. Y. Tam, and S. L. He, "High-frequency ultrasonic hydrophone based on a cladding-etched DBR fiber laser," IEEE Photon. Technol. Lett. **20**(8), 548–550 (2008).
13. B. O. Guan, H. Y. Tam, S. T. Lau, and H. L. W. Chan, "Ultrasonic hydrophone based on distributed Bragg reflector fiber laser," IEEE Photon. Technol. Lett. **17**(1), 169–171 (2005).
14. M. A. Mirza and G. Stewart, "Multiwavelength operation of erbium-doped fiber lasers by periodic filtering and phase modulation," J. Lightwave Technol. **27**(8), 1034–1044 (2009).
15. G. Stewart, G. Whitenett, K. Vijayraghavan, and S. Sridaran, "Investigation of the dynamic response of erbium fiber lasers with potential application for sensors," J. Lightwave Technol. **25**(7), 1786–1796 (2007).

1. Introduction

Many damage-related structural changes, such as crack initiation and growth, twinning, and fiber breakage, can generate ultrasonic pulses with a typical frequency range between 100 kHz and 1 MHz, which are called acoustic emission (AE). Therefore, AE detection is an

#199265 - $15.00 USD Received 10 Oct 2013; accepted 2 Nov 2013; published 18 Nov 2013

important and powerful tool for structural health monitoring. Traditional AE sensors are based on piezoelectric materials. Fiber-optic ultrasonic sensors, particularly those based on fiber Bragg gratings (FBGs) [1–4], offer many advantages compared to their electronic counterpart. They are small, lightweight, durable, immune to electromagnetic interference, and can be easily embedded into structure with little impact on the mechanical properties of the structure. The FBG sensors rely on detecting the spectral shift of the Bragg wavelength caused by the AE signal, typically using lasers, whose wavelength is set to the center of the linear range of the FBG reflection spectrum, to perform intensity-based sensor demodulation. Obviously, the detection sensitivity is dependent on the slope of the FBG reflection spectrum, which is relatively wide. Although narrower spectrum can, in theory, be obtained by ultra-long FBGs, the detection sensitivity is significantly reduced when the grating length and the ultrasonic wavelength become comparable [5]. Tsuda developed a simple fiber-ring laser (FRL) ultrasonic sensor in which a FBG is included in the laser cavity and used as the sensing element [6, 7]. The FRL lases at the Bragg wavelength of the FBG. Due to the wavelength dependence of the optical gain of the erbium-doped fiber (EDF) in the laser cavity, the FBG spectral shift is converted to laser intensity variations. However, the gain medium only shows small and uncontrollable wavelength dependence, so that the sensitivity is low. Recently, ultrasonic sensors based on π-phase-shifted FBGs (πFBG) have attracted a great deal of attention for highly-sensitive ultrasonic detection [5, 8–10]. A πFBG can be conceptually considered as a Fabry-Perot cavity formed by two grating mirrors. When the grating is highly reflective, the π-phase shift at the center of the grating structure leads to an extremely narrow notch in the reflection spectrum even for short grating length, leading to much improved sensitivity. The sensors can be demodulated using the Pound-Drever-Hall method or by a laser source whose frequency needs to be set within the linear range or around the center of the πFBG spectrum. Both require the use of a narrow-linewidth tunable laser to follow the low-frequency spectral shift from quasi-static strain signals. The high cost of tunable lasers makes the sensor system less attractive in practical applications. Using the beat frequency of the two polarization modes of a distributed Bragg reflector laser is a promising method for ultrasonic detection in a liquid environment and has been extensively studied in the past few years [11–13]. This method is based on the beat frequency change from the anisotropic modification to the fiber refractive index caused by an ultrasonic wave whose wavelength is smaller than or comparable to the fiber diameter. However, it may not be suitable for detection of AE signals that have a much lower frequency range.

Here, we propose and investigate a novel FRL sensor system that incorporates a regular FBG and a narrow tunable optical band-pass filter (TOBPF) in the laser cavity loop for sensitive ultrasonic detection. In this approach, the regular FBG is the sensing element that modulates the cold-cavity loss of the fiber-ring laser according to the ultrasonic signal and the TOBPF, whose bandwidth is much narrower than that of the FBG, is used to ensure that the FRL lases at a point on the spectral slope of the FBG. Compared to conventional laser-demodulated passive FBG sensors, our theoretical analysis shows that the proposed method is much more sensitive. In addition, the proposed system has a very simple structure and the ultrasonic signal can be directly detected by monitoring the power fluctuations of the laser output using a photodetector (PD). Therefore, the system is potentially low cost.

2. Theory

2.1 Principle of operation

The schematic of the proposed FRL ultrasonic sensor system is shown in Fig. 1(a). The gain medium is an EDF pumped by a 980 nm laser diode through a 980/1550 nm wavelength division multiplexer (WDM). A fiber-optic isolator is used to ensure that the lasing only occurs at one direction around the loop. A regular FBG, which is the sensing element, is incorporated into the laser cavity through a fiber-optic circulator. A narrow TOBPF is included in the main loop of the laser cavity. Figures 1(b) and 1(c) are, respectively, the schematics of the reflection spectrum of the FBG and the transmission spectrum of the

#199265 - $15.00 USD Received 10 Oct 2013; accepted 2 Nov 2013; published 18 Nov 2013

TOBPF. Their spectra are designed to ensure that the FRL only lases at the wavelength defined by the narrow transmission peak of TOBPF. Note that the wavelength of the TOBPF transmission peak is slightly off the center of FBG reflection spectrum. When an ultrasonic signal impinges onto the FBG, it causes the FBG spectral shift that follows the instantaneous strength of the ultrasonic signal. Because of the FBG spectral slope at the laser wavelength, the effect of the ultrasonic signal is to modulate the cold cavity loss of the FRL. As a result, the output optical power of the FRL fluctuates according to the loss modulation. Therefore, the ultrasonic signal can be detected from the variations of the laser output power, which is measured by a PD. Due to the use of the TOBPF, the proposed FRL sensor system can also adapt to the large FBG spectral shift caused by low-frequency strains applied to the FBG by locking the TOBPF wavelength to the operational point on the spectral slope.

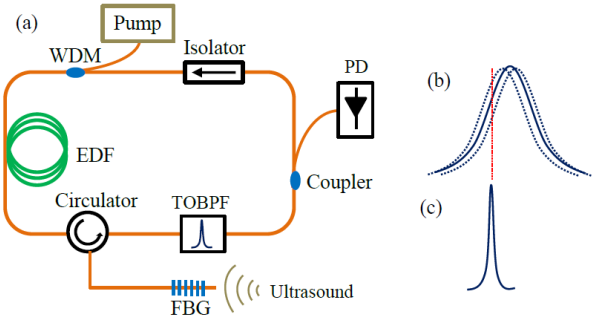

Fig. 1. Schematic of (a) the proposed FRL ultrasonic sensor system; (b) the reflection spectrum of the sensing FBG and the effect of the ultrasonic signal on the spectrum; and (c) the transmission spectrum of the TOBPF.

2.2 Numerical simulation

Numerical simulation is performed to verify the ultrasonic detection method proposed here. The operation of the FRL is modeled by a set of rate equations following the model described in [14, 15]. More specifically, the EDF is described by a two-level model in which the gain from the EDF is assumed to be proportional to a uniform, length-averaged inversion level, $N_2(t)$. The laser output contains a large number of longitudinal modes that are divided into G groups that are equally-spaced in the frequency domain. Each mode group contains m longitudinal modes all of which have identical parameters. Assuming the number of photons in the g^{th} mode group counted at the output of the EDF is $M_g(t)$, the equation describing the rate of changes of $N_2(t)$ given in [14] is reproduced here:

$$(\rho Sl)\frac{dN_2}{dt} = P_p\left(1-e^{g_p l}\right)-(\rho Sl)\frac{N_2}{\tau_0}-\sum_{g=1}^{G}\frac{M_g}{\tau}\left(1-e^{-g_g l}\right)-R_{ASE}, \qquad (1)$$

where t denotes time, ρ is the erbium-ion density, S and l are, respectively, the core cross-sectional area and the length of the EDF, τ_0 is the lifetime of the upper state, τ is the round trip time of the laser cavity, P_p is the pump power in unit of photons/second, $g_p = -\alpha_p(1-N_2)$ is the length-averaged pump absorption coefficient, and $g_g = (\gamma_g + \alpha_g)\, N_2 - \alpha_g$ is the length-averaged gain coefficient for the g^{th} mode group. Here, α_p is the absorption coefficient of the EDF at the pump wavelength, and γ_g and α_g are, respectively, the emission and absorption coefficients of the EDF at the wavelength of the g^{th} mode group. The round trip time, τ, is related to the round-trip cavity length, L, and the effective refractive index of the fundamental mode, n, by $\tau = nL/c$, where c is the light speed in vacuum. The term of R_{ASE} in Eq. (1) corresponds to the rate of change of $N_2(t)$ caused by the amplified spontaneous emission (ASE) and is given by

$$R_{ASE} = \sum_{g=1}^{G} 4m\frac{\gamma_g l N_2}{\tau}\left(A_g - 1\right), \qquad (2)$$

#199265 - $15.00 USD Received 10 Oct 2013; accepted 2 Nov 2013; published 18 Nov 2013

where $A_g = \left(e^{g_g l} - 1\right) \Big/ g_g l$ is the ASE amplification factor for the g^{th} mode group. The equation for the rate of change of $M_g(t)$ is also reproduced here:

$$\frac{dM_g}{dt} = \frac{M_g}{\tau}\left(G_{fg} e^{g_g l - \alpha_c} - 1\right) + P_{ASEg}, \tag{3}$$

where α_c is the cold cavity loss (loss external to the EDF) excluding the FBG and the TOBPF. The loss from the FBG and the TOBPF is a function of the laser wavelength (group number) and is represented by G_{fg}. The term of P_{ASEg} is related to the ASE and is given by

$$P_{ASE} = \frac{2m}{\tau} \gamma_g l N_2 A_g. \tag{4}$$

Assuming the transmission spectrum of the TOBPF is Gaussian with a bandwidth much narrower than the reflection bandwidth of the FBG, the loss from the TOBPF and the FBG without the ultrasonic signal can then be written as

$$G_{fg} = R_0 \exp\left[-\left(\frac{\lambda - \lambda_0}{\Delta\lambda}\right)^2\right], \tag{5}$$

where λ denotes wavelength, λ_0 is the center wavelength of the TOBPF, $\Delta\lambda$ represents the half-width at $1/e$ maximum of the TOBPF transmission spectrum, and R_0 is the reflectivity of the FBG at wavelength λ_0. The ultrasonic signal causes small shifts of the FBG reflection spectrum. Because the TOBPF spectrum is much narrower than the FBG spectrum, it can be assumed that the lasing wavelength does not change with the FBG spectral shift. The effect of the ultrasonic signal is to provide a modulation to R_0 that is proportional to the ultrasonic signal. With presence of the ultrasonic signal, Eq. (5) becomes

$$G_{fg} = R_0 \exp\left[-\left(\frac{\lambda - \lambda_0}{\Delta\lambda}\right)^2\right]\left[1 + k\delta\lambda_m \sin\left(2\pi f t\right)\right], \tag{6}$$

where f is the ultrasonic frequency, $\delta\lambda_m$ is the magnitude of the spectral shift caused by the ultrasonic signal, and k is the spectral slope of the FBG at wavelength of λ_0.

The Runge-Kutta method is employed to solve the set of rate equations. The parameters used for the EDF, which operates at the wavelength of 1550 nm, are given as follows: $\rho = 2 \times 10^{24}$ ions/m^3, $S = 8.04$ μm^2, $l = 3$ m, $\tau_0 = 10.2$ ms, $\alpha_p = 4.64$ dB/m, $\alpha_e = 3.00$ dB/m, and $\gamma = 3.70$ dB/m. The parameters for the rest of the laser system are: $\alpha_c = 8$ dB, $L = 15$ m, $n = 1.456$, $\Delta\lambda = 20$ pm, $R_0 = 0.8$, and P_p corresponds to a pump power of 100 mW at wavelength of 980 nm. To simulate the response of the sensor system to ultrasonic signals, first, a step input is used for the pump power at $t = 0$ and Eqs. (1)-(5) are solved to obtain the evolution of $N_2(t)$ and $M_g(t)$ until they reach steady states. Then the steady-state solutions of $N_2(t)$ and $M_g(t)$ are used as the initial conditions to solve the rate equations when the FBG is subject to the ultrasonic signal, in which Eq. (5) is replaced by Eq. (6). The output signal from the PD is proportional to the laser power at the output of the EDF, P_{out}, which is the sum of the power of all mode groups:

$$P_{out} = \frac{hc}{\lambda\tau} \sum_{g=1}^{G} M_g, \tag{7}$$

where h is the Planck's constant.

We first analyze the sensor response to a continuous sinusoidal ultrasonic signal with a frequency of 200 kHz. The continuous signal starts from $t = 0$ and is truncated at $t = 4.77$ ms. It is assumed that the amplitude of the spectral shift induced by the ultrasonic signal is $\delta\lambda_m = 0.1$ pm and the spectral slope of the FBG at the lasing wavelength is $k = 5$ nm^{-1}. Figure 2(a)

#199265 - $15.00 USD Received 10 Oct 2013; accepted 2 Nov 2013; published 18 Nov 2013

shows the laser power in the time domain when it reaches steady-state. It is a sinusoidal signal with the same frequency as the ultrasonic signal and a dc power level of 32.37 mW. The amplitude of the signal is ~0.22 mW, corresponding to a change of 6.8×10^{-3} relative to the laser output power. Recalling that the spectral slope of the FBG is 5 nm^{-1} and the amplitude of the spectral shift is 0.1 pm, a conventional passive laser-based demodulation of the FBG can only yield an amplitude change of 5×10^{-4} relative to the laser power. Therefore, the sensitivity of the proposed fiber-ring laser system with these particular parameters is more than 10 times higher than the conventional passive demodulation system. Figure 2(b) is the spectrum obtained by the Fourier transform of the laser output power. There are three peaks in the spectrum. The strongest peak is at 200 kHz and clearly indicates that the FRL sensor provides a response with the same frequency to the ultrasonic signal. The peak at 400 Hz is the second-order harmonic signal which is believed to originate from the nonlinear nature of the laser operation. The harmonic signal is very weak with an amplitude almost 60 dB lower than the signal peak at 200 kHz. Finally, the peak at 86 kHz is associated with the relaxation-oscillation of the FRL and caused by the transient process when the FRL is disturbed from its steady state by the ultrasonic signal. Relaxation oscillation can be a major noise source in practical applications. Because the frequency of the AE signal typically is larger than 100 kHz, the relaxation oscillation noise can be effectively removed by an electric filter.

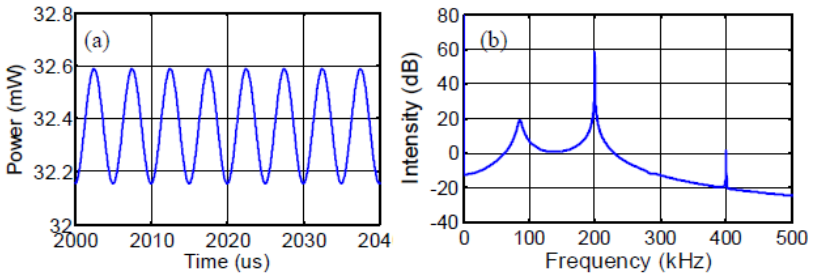

Fig. 2. (a) Simulated sensor response to a 200 kHz continuous sinusoidal ultrasonic signal; (b) spectrum of the sensor response.

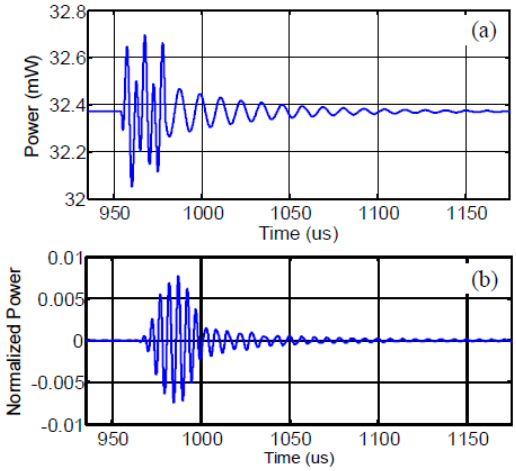

Fig. 3. Simulated sensor response to a 5-cycle 200 kHz ultrasonic pulse: (a) signal before the digital BPF and (b) signal after the digital BPF.

The proposed system is further investigated by simulating its response to an ultrasonic pulse. In this case, the ultrasonic pulse is a 200 kHz sinusoidal signal with only 5 cycles. The same peak wavelength shift ($\delta\lambda_m$ = 0.1 pm) and the spectral slope (k = 5 nm^{-1}) of the FBG

#199265 - $15.00 USD Received 10 Oct 2013; accepted 2 Nov 2013; published 18 Nov 2013

spectrum are assumed. Figure 3(a) shows the laser output power in the time domain in response to the ultrasonic pulse. It is seen that the sensor response resembles a superposition of the 200 kHz signal of interest and a relaxation oscillation. To remove the relaxation oscillation, a digital band-pass filter from 140 kHz to 300 kHz is applied to the signal and the result (normalized to the dc laser power) is shown in Fig. 3(b), resulting in a signal more resembling the ultrasonic pulse. The peak variation of the signal is 7.5×10^{-3}, which is close to the result obtained for the case of the continuous sinusoidal ultrasonic excitation.

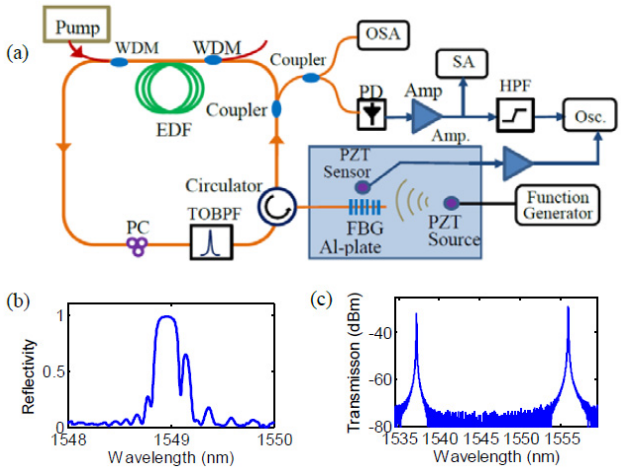

Fig. 4. (a) Schematic of the experiment set up; (b) normalized reflection spectrum of the sensing FBG calculated from the measured transmission spectrum; and (c) measured transmission spectrum of the TOBPF. PC: Polarization controller; Osc.: Oscilloscope.

3. Experiment

The proposed FRL sensor system was experimentally demonstrated for ultrasonic detection using an experimental setup shown in Fig. 4(a). Compared to Fig. 1(a), an extra 980/1550 nm WDM was used to guide the residual power from the 980 nm pump laser out of the FRL cavity. The length of the EDF (Model: I-6, Fibercore, UK) was ~3 m. The sensing FBG was 7 mm long and was fabricated using the phasemask method and a 193 nm excimer laser. A TOBPF (Model: FFP-TF2, Micron Optics) with a 3-dB bandwidth of ~27 pm for the transmission peak was used in the laser cavity loop. It is based on a high-finesse Fabry-Perot interferometer and has an all-fiber structure. The wavelength of the TOBPF can be electronically-tuned by a voltage signal through a build-in PZT and, according to the product specification, the maximum tuning speed is 800 Hz over one free-spectral range (FSR ~20 nm for the TOBFP). With such high wavelength tuning speed, the TOBFP can also be used to lock the lasing wavelength to the optimized position on the spectral slope of the sensing FBG to compensate for the low frequency spectral shift caused from the temperature variations and quasi-static strain. The reflection spectrum of the FBG, which was calculated from its transmission spectrum measured by an optical spectrum analyzer (OSA), and the transmission spectrum of the TOBPF (when no-voltage was applied for tuning) are shown in Figs. 4(b) and 4(c), respectively. The loss of the TOBPF at the transmission peaks was measured to be ~3 dB. Due to the potential polarization-dependence loss from the components in the laser cavity, a fiber-optic polarization controller was included in the cavity to adjust the laser polarization. The total length of the fiber cavity was estimated to be ~15 m. The light was partially coupled out of the laser cavity through a 33/67 fiber coupler, which was followed by another 20/80 fiber coupler to simultaneously monitor the optical spectrum using an OSA and the laser power using a PD. The signal from the PD was then amplified by a 35-dB amplifier with a bandwidth from 20 kHz to 1.2 MHz followed by a 150 kHz high-pass filter (HPF) to remove the relaxation oscillation and other low frequency noises. The spectrum of the signal

#199265 - $15.00 USD Received 10 Oct 2013; accepted 2 Nov 2013; published 18 Nov 2013

after the amplifier was measured by an electric spectrum analyzer (SA) and the signal after the HPF was displayed on a digital oscilloscope. The FBG was bonded on a 2′ × 2′ aluminum plate using a general-purpose adhesive (Model: M-Bond 200, Micro-Measurements). A piezoelectric transducer (PZT) (Model: HD-50, Physical Acoustic Corporation) powered by a function generator was used as the ultrasonic source and another PZT (Model: R15α, Physical Acoustic Corporation) was used as a reference sensor that is placed near the FBG on the plate to monitor the ultrasonic signal for comparison with the signal from the FRL sensor system.

We first tested the sensor system for detection of ultrasonic pulses generated from the source PZT powered by a repeating 20 V peak-to-peak burst signal with 5 burst counts and a center frequency of 200 kHz. To study the effect of the FBG spectral slope on the sensor output, the lasing wavelength, which is determined by the center wavelength of the TOBPF, was tuned by a dc voltage signal applied on the built-in PZT of the TOBPF. Figures 5(a)-5(c) are the signals displayed on the oscilloscope for three cases where the TOPBF was tuned to three different wavelength positions and Fig. 5(e) shows their corresponding laser spectra relative to the FBG reflection spectrum that is shown in Fig. 5(d). The signals detected by the PZT sensor are also shown in Figs. 5(a)-5(c). The results from both sensor systems are similar and clearly indicate that the FRL system successfully detected the ultrasonic signal. Note that the signals from both sensors exhibit a series of wave packets. The first one with the largest amplitude corresponds to the ultrasonic pulse that directly impinged onto the sensors and the following ones correspond to the ultrasonic pulses due to the reflections from the edges of the aluminum plate. The signal from the FRL sensor system shown in Fig. 5(a) has the largest amplitude and best signal-to-noise ratio among all three cases and agrees well with the simulated results shown in Fig. 3(b). The lasing wavelength for this case was 1548.6 nm, as shown by the blue curve in Fig. 5(e). As expected, the FBG reflection spectrum exhibits a large spectral slope at this wavelength. When the lasing wavelength moved to positions of smaller spectral slopes of the FBG spectrum, indicated by the red and black curves in Fig. 5(e), the signal amplitude becomes proportionally smaller, as shown in Figs. 5(b) and 5(c), although the lasing power is higher due to the larger reflectivity of the FBG at these wavelengths.

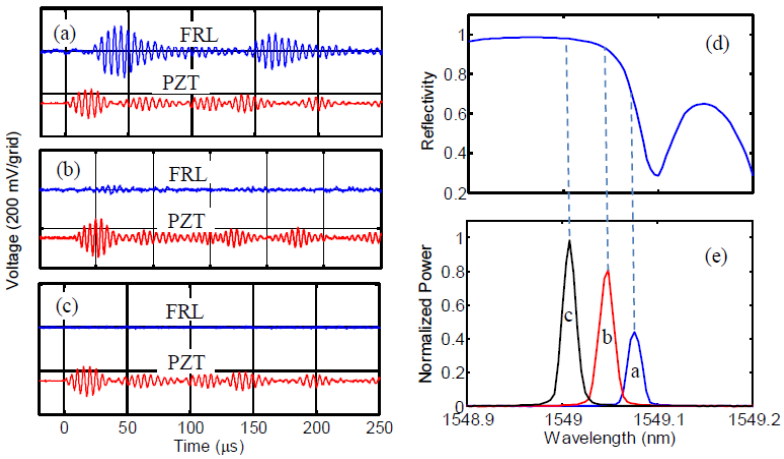

Fig. 5. (a-c) Responses from the FRL sensor system and the PZT sensor system to a ultrasonic pulse when the lasing wavelength was tuned to different positions on the slope of the FBG reflection spectrum (for clarity, the signals from the PZT are normalized and shifted in the vertical axis); (d) the FBG reflection spectrum; and (e) the lasing wavelengths corresponding to (a-c) and relative to the FBG spectrum shown in (d).

We then tested the response of the sensor system to continuous sinusoidal ultrasonic signals. In this experiment, the source PZT was powered by a 200 kHz continuous signal with a peak-to-peak voltage of 20 V. The results from the FRL sensor system and the PZT sensor

#199265 - $15.00 USD Received 10 Oct 2013; accepted 2 Nov 2013; published 18 Nov 2013

system displayed on the oscilloscope are shown in Fig. 6(a). Again, they agree well with each other. Figure 6(b) shows the spectrum of the signal from the PD after the amplifier with a bandwidth range of 20 kHz-1.2 MHz but before the HPF measured by the SA. The measured spectrum is similar to the result obtained from the numerical simulation shown in Fig. 2(b). The strong peak corresponding to the 200 kHz signal is clearly shown in the measured spectrum. Several noise peaks ranging from 20 to 70 kHz that correspond to the relaxation oscillation are also evident. As predicted by the simulation, the experimentally-measured spectrum also shows a small second-order harmonic peak at 400 kHz whose intensity is ~70 dB below the signal peak at 200 kHz.

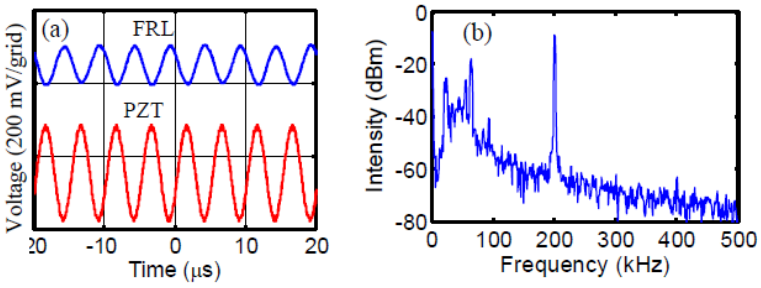

Fig. 6. (a) Signals recorded by the oscilloscope from the FRL sensor system and the PZT sensor system when the sensors were applied to a 200 kHz continuous sinusoidal ultrasonic signal (for clarity, the signal from the PZT is normalized and shifted in the vertical axis) and (b) Spectrum recorded by the SA for the amplified RFL output signal.

4. Summary

We have theoretically and experimentally demonstrated a fiber-optic ultrasonic sensor based on a FRL that contains a regular sensing FBG and a TOBPF in the laser cavity. The lasing wavelength is set on the spectral slope of the FBG by the TOBFP. The ultrasonic signal is detected by the laser power variations in response to the cold-cavity loss modulations from the ultrasonically-induced FBG spectral shift. A theoretical model and an experimental setup have been established to verify the operation of the sensor system. The results from the simulation and the experiment agree well with each other. In practical applications where the FBG experiences large and low-frequency spectral shifts caused by quasi-static strains or ambient temperature variations, the TOBFP can also tune the lasing wavelength to follow these low-frequency shifts and ensure the FRL operates at the optimal operational point. Due to the simple structure and the intensity-based demodulation, the system demonstrated here is attractive for AE detections in structural health monitoring. Future research will be focused on experimentally characterizing system performance and using the model developed here to study the effect of the key FRL parameters, such as the laser cold-cavity loss, the laser cavity length, the FBG spectral slope, the length and doping levels of the EDF, and the pump power, on the performance of the sensor system.

Acknowledgments

This work was supported by the Office of Naval Research under grants N000141310159 and N000141110262, and the National Science Foundation under grant EPS-1004094.